Wavelength-selective pyroelectric THz detectors

Christopher Arose[1], Anthony C. Terracciano[2,3], Robert E. Peale[1], Subith S. Vasu[2,3]

[1.] Department of Physics, University of Central Florida, Orlando, FL
[2.] Department of Mechanical and Aerospace Engineering, University of Central Florida, Orlando, FL
[3.] Center for Advanced Turbomachinery and Energy Research, University of Central Florida, Orlando, FL 32816

Abstract

Pyroelectric lithium tantalate (LT) wafers were integrated with sub-wavelength resonant absorbers for spectral sensing at THz frequencies. Devices were designed using electrodynamic simulation. A periodic surface pattern of gold resonators was patterned on the surface of thin LT wafers by photolithography, using a Ti sticking layer. Reflectivity was characterized using vacuum-bench Fourier transform reflectance spectroscopy down to 0.3 THz using a globar source, mylar pellicle beamsplitters, and liquid helium-cooled bolometer at 4 K. Photoresponse was measured using a blackbody and a tunable mm-wave source, with the detector thermally isolated in a vacuum box with polyethylene window. The spectra reveal a pair of absorption bands separated by 0.30 to 0.45 THz. The maximum absorption varies between 30 and 70 % as a function of design parameters. The resonances are insensitive to incidence angle or polarization. Experimental results agree with design predictions. The sticking layer used for gold adhesion was found by the simulation to shift the resonance frequencies by up to 7%, to decrease the maximum absorption, and to broaden the resonances. The LT thickness of 50 micron was chosen to be thin enough to have low thermal mass but thick enough to be handled during processing. However, some of the responses can be attributed to Fabry-Perot resonances when the wavelength in LT becomes comparable to the LT thickness, so a more spectrally pure response would be achieved by avoiding those thicknesses.

1. INTRODUCTION

The THz regime is a section of the electromagnetic spectrum for which historically it has been difficult to engineer effective devices, typically due to low source power focused in the THz, and lack of natural materials that absorb in this frequency range. Advances in technology have led to increased interest in the THz regime, and it is now under intense study for its potential uses in spectroscopy, lasing technology, and imaging, among other applications [1-3]. Of particular interest is selective detection for the ability to detect specific substances by their unique THz spectra [4]. Some devices proposed for this purpose are time-intensive to manufacture [5] or introduce angular dependence [6, 7]. Angular dependence may be detrimental to real-world applications, such as standoff detection, like that used by law enforcement agencies. Here, we demonstrate a detector design made with a single optical lithography step and an angle-independent response [8].

Spectrally selective detectors typically utilize some form of the selective absorber layer, which is engineered for specific resonant frequencies [5, 9, 10]. This film is made of a layer of highly conductive material that is very thin compared to the underlying detector element, with periodic structures that are smaller than the desired detection wavelength [11, 12]. Many patterns have been proposed for use in this layer, such as split-ring resonators, Salisbury screens, and metal patches [13-15]. These layers function by promoting a plasmonic resonance in the metal film that concentrates the electromagnetic energy and then couples the disappeared heat into the detecting element. The materials and geometry are used to define the spectral characteristics of the resonances.

2. METHODS

The absorber pattern used for this detector was adapted from earlier investigations [16-18]. The detectors were fabricated on 50 µm thick z-cut LT wafers. Figure 1b illustrates absorber parameters and Fig. 1c depicts the layer stack of a detector. Contact photolithography was used along with e-beam evaporation to fabricate the detectors. A 100nm Ti/Au layer was used both for the absorber layer and for the metal backplane. An optical lithography mask with 25 patterns was

used for this project to test the absorption characteristics of multiple absorber dimensions. The patterns in Fig 1a are used to refer to specific absorber patterns used for detectors.

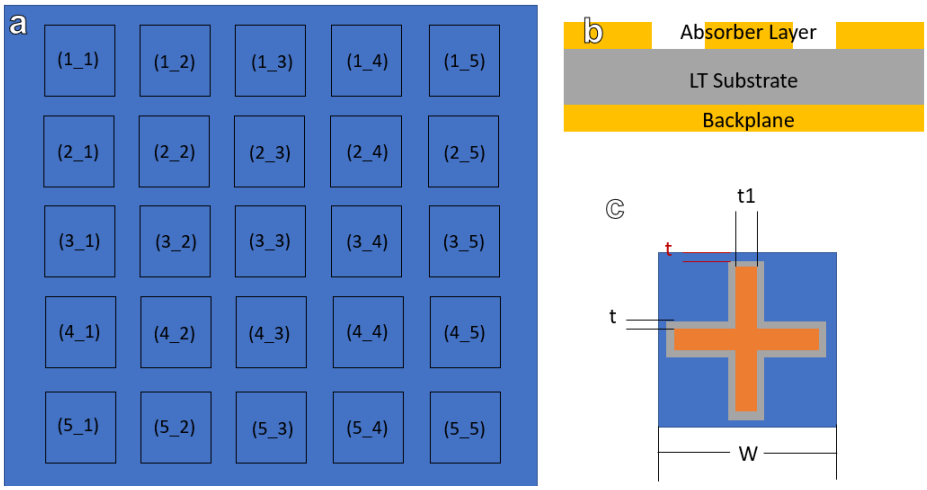

Figure 1: (a) Optical Lithography mask pattern layout. (b) Detector layer stack. (c) Single absorber schematic.

Finite-element simulations were run in CST Microwave Studio Suite 2019 with Drude-model permittivity spectra for gold and titanium and a Lorentz dispersion model used for the LT permittivity. Periodic boundary conditions and a linearly polarized excitation signal were used.

Reflectance measurements were performed in a Bomem DA8 FTIR with a reflectivity rig having 8° incidence angle with respect to the detector surface normal. A gold mirror was used as a reference. The setup is illustrated in Fig 2a. A range of mylar pellicle beamsplitters, a globar source, and a liquid helium-cooled Si bolometer (IR labs) was used.

Responsivity measurements were taken with a Virginia Diodes THz multiplier system with an HP8350b used as the excitation source. The sample was placed in the path of the THz source with a high-density black polyethylene filter in place to block any stray radiation from lab lights or equipment, and the signal was fed into a Stanford Research SR560 low noise voltage preamp, then into a Stanford Research SR530 lock-in amplifier. The setup for these measurements and those taken with the blackbody are illustrated in Fig 2b.

D* measurements were taken by measuring detector response to a blackbody source with a black polyethylene filter. The signal was fed into the same setup like that for the responsivity measurements. The incident power was calculated from the in-band radiance, blackbody aperture area, and solid angle subtended by the detector from the blackbody aperture. The spectral noise density was measured on an HP3582A spectrum analyzer and used to calculate the D*.

Response under vacuum was measured by placing the samples in a custom windowed vacuum housing, which was pumped to 10^{-5} Torr with a turbopump, then sealed. The vacuum was then turned off to minimize any mechano-acoustic noise.

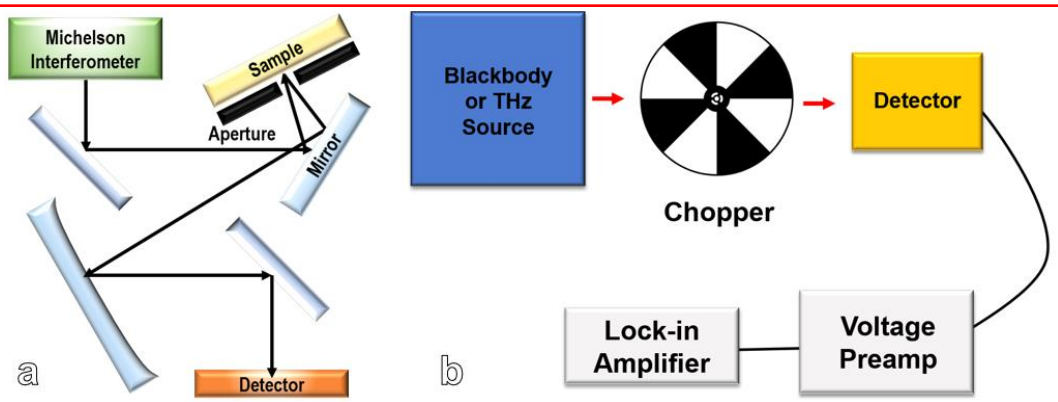

Figure 2: (a) beam path for reflectivity measurements in FTIR. (b) Experimental setup for responsivity and blackbody measurements.

3. RESULTS

Figure 3a presents the measured and simulated reflectance spectra for pattern 3_4. The simulation sticking layer (red line) has poor overlap with the measured absorption. The difference between reflectance minima is 16%. Including the titanium sticking layer improves the agreement, giving a percent difference of reflectance minima of 8%.

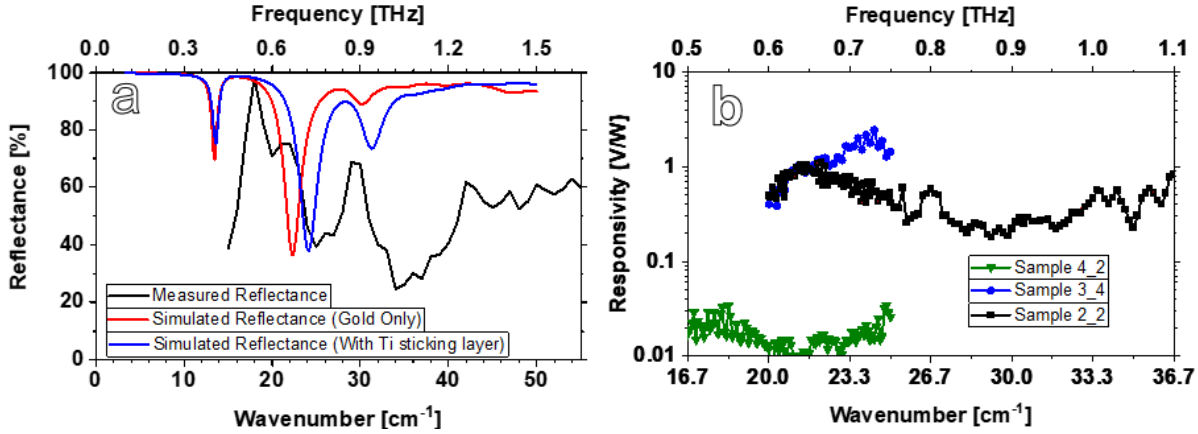

Figure 3: (a) Comparison of measured reflectance to simulations with and without the titanium sticking layer accounted for pattern 3_4. (b) Responsivity plot of detectors.

The responsivity spectrum for the two patterns tested can be seen in Figure 3b. Pattern 3_4 can be seen to have a responsivity of 2.4 V/W, while pattern 2_2 had a max responsivity of 1.2 V/W. This is partially from the higher absorption that pattern 3_4 has in this frequency range. Another factor could be the quality of the mount to the chip carrier increasing resistance for sample 2_2. The sample with pattern 4_2 had a responsivity on the order of 0.01V/W. This is likely due to a different mounting method used that relied on mechanical contact between the sample and a conductive plate which was then probed by another physical contact probe. Contact was likely poor, which led to low signal measurements. For this reason, this sample was not measured for D*, and only samples mounted to chip carriers were used from this point on.

The compilation of simulated and measured data for pattern 3_4 is presented in Figure 4. The data shows good agreement between simulation and experiment. The responsivity maximum and simulated reflectance minimum align remarkably well at 24.0 and 24.3 cm^{-1} (0.72 and 0.73 THz), respectively, while the measured reflectance minimum is at 26.0 cm^{-1} (0.78 THz), which is within 10% of the other results.

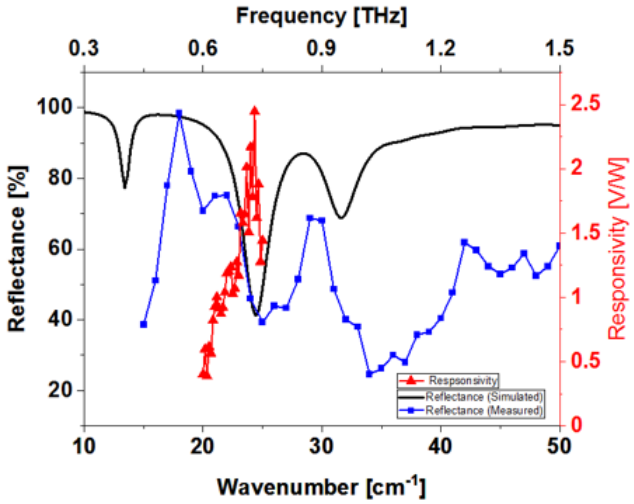

Figure 4: Simulated and measured reflectance plotted against measures responsivity for sample 3_4.

D* is plotted in Figure 5a as a function of chopping frequency and for different degrees of thermal isolation. Two samples with pattern 3_4 were used in this test. One was simply affixed to the chip carrier with conductive silver paint, while the other was fixed on an air bridge made from two pieces of titanium-coated glass. The maximum D* for the non-isolated sample was 1.1×10^5 Jones, while the maximum for the thermally isolated sample was 1.5×10^5 Jones. The difference is starker for higher chopping frequencies, approaching a two-fold increase in D* for the thermally isolated sample. The sample with pattern 2_2 had a maximum D* of 4×10^4 Jones, and pattern 4_2 was not tested here because of its poor responsivity.

To further increase the D* of the detectors, the thermally isolated sample was placed under vacuum, and the same test was run. It can be seen in Figure 5b that the vacuum caused very little difference in the signal seen. The maximum difference in signal was 4%, which could be due to a difference in the quality of detector mounting.

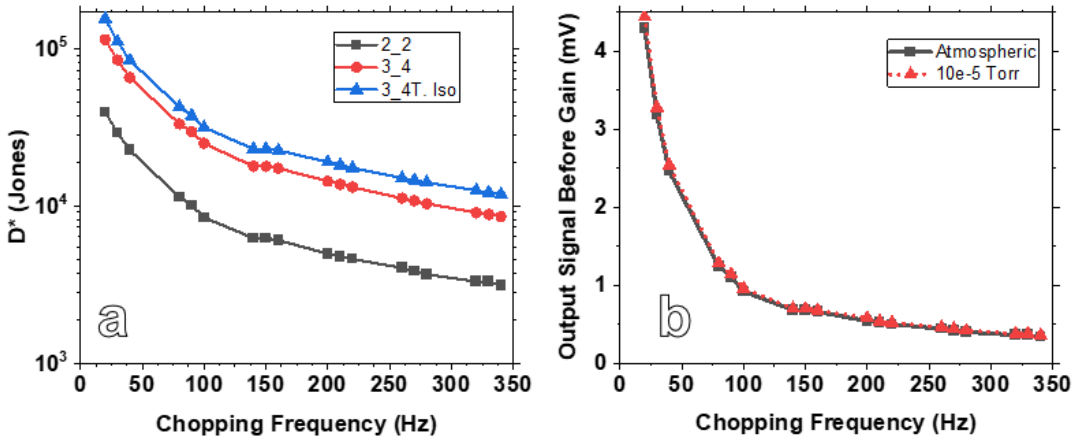

Figure 5: (a) D* of Samples at various chopping frequencies. Sample 3_4 was tested both with and without thermal isolation from its chip carrier. (b) Vacuum test for sample 3_4 thermally isolated.

4. CONCLUSIONS

The considered LT detectors with resonant absorbers show spectral selectivity that is designed tunable. Resonances measured were within 10% of simulated resonances. Responsivities on the order of 1V/W and D* of order 10^5 Jones were measured. Both are orders of magnitude lower than commercial non-selective (?) detectors, but the two-fold increase in D* with a simple air bridge shows promise for further optimizations to be made. One simple optimization

would be operating at a lower chopping frequency, as relatively high frequencies were used in these tests to gauge the response time of the detectors.

ACKNOWLEDGMENTS

This material is primarily based upon work supported by the U.S. Defense Advanced Research Projects Agency (DARPA) via Young Faculty Award # D18AP00040. This work also benefitted from the National Aeronautics & Space Administration (NASA) project # 80NSSC21K1901 and NASA Florida Space Grant Consortium (Award # 80NSSC20M0093).

REFERENCES

1. B-X. Wang, L-L. Wang, G-Z. Wang, W-Q. Huang, X-F. Li, X. Zhai, *Theoretical Investigation of Broadband and WIde-Angle Teraherts Metamaterial Absorber.* IEEE Photonics Technology Letters, 2014. **26**.
2. H. Feng, et al, *Tunable polarization-independent and angle-insensitive broadband terahertz absorber with graphene metamaterials.* Optics Express, 2021. **29**.
3. R. Szipocs, A. Kohazi-Kis, P. Apai, E. Finger, A. Euteneuer, M. Hofmann, *Spectral filtering of femtosecond laser pulses by interference filters.* APpl. Phys. Lett. B, 2000. **70**.
4. W.D. Zhang, A.Bykhovski, L.S. Himed, E.R. Brown, *Spectroscopic Sensing of Opioids in the THz Region*, in *IEEE National Aerospace and Electronics Conference*. 2019, IEEE: Dayton, OH.
5. A. Ebrahimi, R.T. Ako, W.S.L. Lee, M. Bhaskaran, S. Sriram, and W. Withayachumnankul *High-Q Terahertz Absorber With Stable Angular Response.* IEEE transactions on Terehertz Science and Technology, 2020. **10**.
6. A. Datta, Z. Zeng, X. Xu, *Split ring resonator as a nanoscale optical transducre for heat-assisted magnetic recording.* Optics Express, 2019. **27**.
7. J. Le Perchec, R.E. Lemaestre, M. Brun, N. Rochat, O. Gravrand, G. Badano, J. Hazart, S. Nicoletti, *High rejection bandpass optical filters based on sub-wavelength metal patch arrays.* Optics Express, 2011. **19**(17).
8. C. Arose, A.C. Terracciano, R.E. Peale, S.S. Vasu, *Selective Terahertz Absorber for Angle and Polarization-Independent Spectral Sensing.* Optics Letters, 2022.
9. D. Zhai, R. Zhao, Z. Geng, B. Cui, Y. Yang, *A High-Selectivity THz Band-Stop Filter Based on a Flexible Polymide Film.* SPIE, 2018. **10826**.
10. S. Barzegar-Parizi and A. Ebrahimi, *Ultrathin, polarization-insensitive multi-band absorbers based on graphene metasurface with THz sensing application.* Journal of the Optical Society of America B, 2020. **37**.
11. J. Talghader, A. Gawarikar & R. Shea, *Spectral selectivity in infrared thermal detection.* Light Sci Appl, 2012. **1**.
12. T. Ebbesen, H. Lezec, H. Ghaemi, et al, *Extraordinary optical transmission through sub-wavelength hole arrays.* Nature, 1998. **391**: p. 6677-669.
13. A. N. Reddy, S. Raghavan, *Split ring resonator and its evolved structures over the past decade.* IEEE International Conference On Emerging Trends in Computing, Communication, and Nanotechnology, 2013.
14. J. Nath, S. Modak, I. Rezadad, D. Panjwani, F. Rezaie, J.W. Cleary, R.E. Peale, *Far-infrared absorber based on standing-wave resonances in metal-dielectric-metal cavity.* Optics Express, 2015. **23**(16).
15. J. Nath, E. Smith, D. Maukonen, R.E. Peale, *Optical Salisbury screen with design-tunable resonant absorption bands.* Journal of Applied Physics, 2014. **115**.
16. C. Arose, A.C.T., R.E. Peale, F.J. Gonzalez, Z. Loparo, J. Cetnar, S.S. Vasu *Far-infrared spectrally selective LiTaO3 and AlN pyroelectric detectors using resonant subwavelength metal surface structures.* MRS Advances, 2020. **5**(31-32).
17. A.C. Terracciano, C. Arose, S.S. Vasu, *Ultra-Spectrally Selective THz Band Stop Reflector*. 2021: United States of America.
18. A.C. Terracciano, R.E. Peale, C. Arose, S.S. Vasu, *Ultra-Spectrally Selective THZ Pyroelectric Detector*. (Pending), 2020.